



Publication Year	2015
Acceptance in OA	2020-03-20T11:01:54Z
Title	Enhancing the efficiency of solar concentrators by controlled optical aberrations: Method and photovoltaic application
Authors	GIANNUZZI, ALESSANDRA, DIOLAITI, EMILIANO, LOMBINI, MATTEO, DE ROSA, ADRIANO GIUSEPPE, MARANO, BRUNO, BREGOLI, Giovanni, Cosentino, Giuseppe, FOPPIANI, ITALO, SCHREIBER, LAURA
Publisher's version (DOI)	10.1016/j.apenergy.2015.01.085
Handle	http://hdl.handle.net/20.500.12386/23432
Journal	APPLIED ENERGY
Volume	145

Enhancing the efficiency of solar concentrators by controlled optical aberrations: method and photovoltaic application

Alessandra Giannuzzi^{1*}, Emiliano Diolaiti¹, Matteo Lombini¹, Adriano De Rosa², Bruno Marano³, Giovanni Bregoli¹, Giuseppe Cosentino³, Italo Foppiani¹ and Laura Schreiber¹

¹INAF-Osservatorio Astronomico di Bologna, Via Ranzani 1, I-40127 Bologna, Italy

²INAF-Istituto di Astrofisica Spaziale e Fisica Cosmica, Bologna, Via P. Gobetti 101, I-40129 Bologna, Italy

³DIFA-Dipartimento di Fisica e Astronomia, Alma Mater Studiorum Università di Bologna, Via Ranzani 1, I-40127 Bologna, Italy

ABSTRACT

We present a general method, based on controlled static aberrations induced in the reflectors, to boost receiver performances in solar concentrators. Imaging mirrors coupled with dense arrays suffer from severe performance degradation since the solar irradiance distribution is bell-shaped: mismatch losses occur in particular when the cells are series connected. The method consists in computing static deformations of the reflecting surfaces that can produce, for an adopted concentration ratio, a light spot matching the receiver features better than conventional reflectors. The surfaces and the deformations have been analytically described employing the Zernike polynomials formalism. The concept here described can be applied to a variety of optical configurations and collecting areas. As an example, we extensively investigated a dense array photovoltaic concentrator, dimensioned for a nominal power of about 10KWe. The "flat" distribution of light we obtain can exploit the PV device cells close to their efficiency limit. A significant gain is thus obtained, with no need of secondary optics or complex dish segmentation and of special features in the receiver electrical scheme. In the design, based on seven 2.6 m mirrors, we addressed also non-optical aspects as the receiver and the supporting mechanics. Optical and mechanical tolerances are demonstrated not to exceed accurate, but conventional, industrial standards.

KEYWORDS

photovoltaic concentrator (CPV), dense-array receiver, numerical optimization, optical design, Zernike polynomials

1. INTRODUCTION

Concentrating Photovoltaics technology (CPV) is experiencing a growing interest thanks to the development of solar cells with continuously improved efficiency. At present, the best reported cell is a 0.165 cm² multi-junction (MJ) cell having a new record of 44.4% confirmed efficiency at direct irradiance concentration of 302 suns (1 sun = 1000 W/m²) [1]. For both high concentration (HCPV) and low concentration (LCPV) systems the yearly installed capacity increased significantly during the last five years [2]. A simple advantage induced by this technology is that, given the collected energy, the concentration performed by optical devices such as lenses or mirrors allows us to replace the area of photovoltaic material with cheaper optical surfaces. Moreover, high efficiency cells are too expensive to be used in non-concentrating applications. Despite most of the installed systems are point focus lens based as Fresnel [3–6] or micro-dish [7–9] systems, dense array systems have been recently investigated as profitable solutions for lowering the cost per watt-peak supplied [10, 11]. In this technology the light is focused using one large reflective element called dish, onto an array of photovoltaic MJ cells densely packed to form a single detector. If compared with lenses, mirrors have the main advantage to not suffer from chromatic

aberrations. These systems track the sun in two-axis during its daily motion and usually operate in high concentration mode, i.e. with solar flux up to hundreds times the ambient value. Reflective dish concentrators with diameters ranging from few meters to few tens of meters have been already proposed and are at the beginning of their commercial development working at typical concentrations of 500× [12–14].

Traditional dish concentrators have paraboloidal shapes. Theoretically, their diameters could reach several tens of meters as the heliostats in central tower plants, the construction of monolithic mirrors being difficult at these scales. The size generally imposes to approximate the profiles with cheap flat reflecting facets mounted on a common frame and reproducing globally the paraboloidal surface. As for the receivers, standard cells have rectangular shapes and the arrays are groups of cells densely packed together mostly in series and parallels connections. The arrays do consequently resemble rectangular shapes too. When a standard imaging mirror that produces a sun image intrinsically circular is coupled with a rectangular detector problems arise. In this condition some cells could be obscured if the spot is smaller than the receiver, or part of the light could be lost if the detector is smaller than the spot, these two effects contributing to a substantial loss in efficiency. Moreover, the given irradiance distribution is bell-shaped in contrast with the requirement of having all the cells under the same illumination. In

25
26
27
28
29
30
31
32
33
34
35
36
37
38
39
40
41
42
43
44
45
46
47
48
49
50

*E-mail:alessandra.giannuzzi@unibo.it

51 fact, interconnected cells having identical electrical charac- 109
52 teristics and experiencing the same irradiance/temperature 110
53 conditions produce the same amount of output current and 111
54 voltage. Mismatch losses occur instead when interconnected 112
55 cells experience different conditions, in particular for series 113
56 connections. Still few investigations have been specifically 114
57 performed on current mismatches in dense array receivers 115
58 exposed to high concentrations [15–17]. The issue of spatial 116
59 light uniformity is instead widely known for single cell de- 117
60 vices [18–21] and the problem is commonly approached by 118
61 the introduction of secondary optics (SO) [22–24] working 119
62 as homogenizers. The presence of an extra secondary op- 120
63 tics is rather useful to increase the acceptance angle leading 121
64 to a relaxation of tracking and alignment tolerances. How- 122
65 ever, this solution has the disadvantage to increase the sys- 123
66 tem complexity and to add reflection losses, chromatic aber-
67 ration (if refractive) and mechanical problems as alignment,
68 stability or mounting. A useful review on the state of the
69 art of the non-uniformity problem for single cell receivers
70 has been recently published [25]. Few commercial systems
71 and technical data are available on secondary optics embed-
72 ded in dense arrays. Some researches faced the uniformity
73 problem from the receiver point of view, developing new
74 electrical connections [26], embedding different cells in the
75 same array [27] or designing new receivers with radial sym-
76 metry [28].

77 Alternative ways of redesigning the primary collector 125
78 have been poorly investigated but some good results has 126
79 been obtained by Chong et al. [29]. The proposed planar 127
80 faceted concentrator coupled to a dense array has been op- 128
81 timized to give a large uniform illumination over the tar- 129
82 get area with a peak intensity of 391 suns. However, such 130
83 a concentrator is made by several mirrors to be mounted 131
84 and aligned before being orientated with the use of line- 132
85 tilting driving mechanism. Moreover, since the final spot 133
86 is the overlap of the multiple facets reflections, the size and 134
87 the uniformity of the final spot is influenced by projection 135
88 and blocking effects which increase with the distance of the 136
89 facets from the centre of the whole assembly. For this rea- 137
90 son, such a mosaic system is not able to both have big col- 138
91 lecting area and high concentration ratio without embedding 139
92 a high number of facets and high focal distances, as reported 140
93 in similar works [30–32]. In [32] the economical viability 141
94 is however claimed for a specific configuration of faceted 142
95 dense array system since a cost for the output power below 143
96 2 euro/watt has been calculated. 144

97 The strategy we suggest in this paper is to boost the spot 145
98 uniformity by only acting on the primary reflector but using 146
99 monolithic big surfaces and avoiding the dish faceting into 147
100 numerous smaller elements. In the proposed method, the 148
101 shape of the mirrors is analytically described by the Zernike 149
102 polynomials and its optimization is numerically obtained to 150
103 give a non-imaging optics able to produce a quasi-square 151
104 spot, spatially uniform and with prescribed concentration. 152
105 The free-form primary optics, optimized in this way and val- 153
106 idated by a ray tracing software, showed a substantial gain 154
107 in efficiency without the employ of secondary optics. At 155
108 the same time, simple electrical schemes for the receiver are 156

required. The concept has been investigated theoretically 109
modeling a CPV application including a conceptual devel- 110
opment of non-optical aspects as the design of the receiver 111
and of the supporting mechanics. For the proposed method 112
and the specific CPV system developed, a patent applica- 113
tion has been filed in Italy. A preliminary analytical study, 114
considering a residential utility, has been also performed in 115
order to understand the energetic and economic performance 116
of the system [33]. The analysis indicates that the maximum 117
sustainable capital cost of the system ranges between 30000 118
euros and 45000 euros depending on the years which are 119
considered for the return of the investment (10 or 20 years 120
respectively). Further more detailed economical evaluations 121
will be performed during the future constructive phases of 122
the project. 123

2. OPTICAL CONCEPT 124

From an optical point of view there is no need for an ac- 125
curate image at the receiver of a solar concentrator. The op- 126
tical design criteria rather concern with the optimal trans- 127
fer of light between the source and the target chosen. To 128
solve matching issues in concentrators we thought to rein- 129
terpret optical concepts largely used in astronomy, where 130
an accurate image formation is an essential premise for ef- 131
ficient observations. In telescopes, controlled mirrors de- 132
formations are introduced by actuators to balance the opti- 133
cal aberrations that degrade the wavefront coming from an 134
observed source [34–36]. What we developed instead is a 135
sort of "reverse" approach of the astrophysical method: the 136
guideline is to apply deformations (active or static) to the 137
mirrors of the solar collectors to introduce aberrations in the 138
wavefront, thus degrading the solar image and, in the case 139
of a CPV dense array system, focusing a squared spot with a 140
prescribed irradiance. The result would be a better match be- 141
tween the irradiance features and the receiver performance. 142

The technical feasibility of our concept is supported by 143
independent studies and projects involving technology trans- 144
fer processes from the astronomical instrumentation knowl- 145
edge. Single monolithic reflectors suitable for concentrators 146
(3.1 meter wide) have been already realized in a customized 147
furnace at the Steward Observatory Mirror Lab, at the Uni- 148
versity of Arizona [37]. A novel mirror concept based on an 149
active laminate consisting of an ultra-thin (less than 1 mm) 150
and ultra-light carbon-fiber shell bonded to a piezo-ceramic 151
active layer have been recently investigated and manufact- 152
ured with the aim of reducing the cost of active mirrors both 153
in telescopes and concentrators [38–40]. 154

To describe the mirrors shape and to perform the opti- 155
mization for a CPV dish, we used the *Zernike polynomials*, 156
an analytical tool largely employed, especially in optics, to 157
characterize functions and data on a circular domain. They 158
form an orthogonal basis on the unit circle and real surfaces 159
can be represented by linear combinations of them. Every 160
Zernike polynomial consists of three components: a normal- 161
ization factor, a radial component and an azimuthal compo- 162
nent. The radial components are polynomials derived from 163

164 the Jacobi polynomials, whereas the azimuthal component
 165 is sinusoidal. As in the Noll formalism [41], the Zernike
 166 polynomials can be defined in polar coordinates (ρ, θ) :

$$Z_{j_{even}} = \sqrt{n+1} R_n^m \rho \sqrt{2} \cos m\theta \quad (1)$$

$$Z_{j_{odd}} = \sqrt{n+1} R_n^m \rho \sqrt{2} \sin m\theta \quad (2)$$

$$Z_j = \sqrt{n+1} R_n^0(\rho) \quad (3)$$

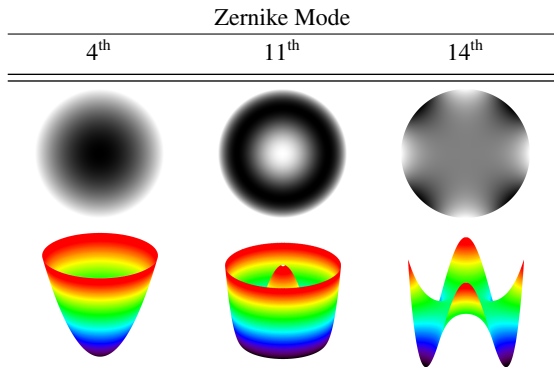
167 where ρ is the normalized radial coordinate ranging from 0
 168 to 1 and θ is the azimuthal angle ranging from 0 to 2π . In
 169 the formulas, m represents the azimuthal frequency and n
 170 the radial degree, both are integer and the condition $m \leq n$,
 171 $n - |m| = \text{even}$ must be satisfied. The index j is a mode
 172 ordering number and is a function of n and m . Equations 1
 173 and 2 exist for $m \neq 0$ while equation 3 for $m = 0$. The double
 174 indexing scheme is useful for unambiguously describing
 175 the functions. In the formulas, $R_n^m(\rho)$ indicates polynomials
 176 with radial dependence.

177 3. CASE OF SINGLE ON-AXIS MIRROR

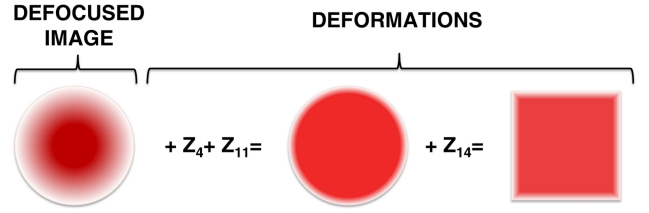
178 An analysis we performed with the ray tracing software
 179 Zemax[®] showed that, starting from a spherical mirror, very
 180 few deformations described by specific Zernike polynomials (modes)
 181 can strongly help in solving the uniformity and shape problem in dense
 182 array receivers. Considering an imaging mirror with deformations,
 183 its surface z (the so-called *sag*) can be approximated by the following
 184 formula:

$$z = \frac{cr^2}{1 + \sqrt{1 - (1+k)c^2r^2}} + \sum_{i=1}^N A_i Z_i(\rho, \theta) \quad (4)$$

185 where N is the number of polynomials, A_i is the coefficient
 186 associated to the i^{th} polynomial, r is again the radial coordinate
 187 in the chosen units, ρ and θ are the polar coordinates
 188 defined before. Eq. 4 depends on the curvature c (which
 189 equals the reciprocal of the curvature radius) and the conic
 190 constant k . The first term in the equation represents an ideal
 191 conic surface (spherical if $k = 0$) while the second term represents
 192 the deformations described by Zernike polynomials. The number of
 193 terms needed for a good surface modeling grows together with the
 194 number of deformations occurring at different scales.
 195



196 **Table 1:** Principal Zernike modes involved in this study.



197 **Figure 1:** Effects introduced on the Sun image by Zernike polynomials 4th, 11th and 14th

198 For a single spherical mirror focusing on axis, we identified
 199 three main polynomials: the 4th, the 11th and the 14th.
 200 Fig. 1 shows how the solar spot produced at a fixed distance
 201 by a spherical mirror can be modified by introducing controlled
 202 deformations related to the three modes here mentioned. This
 203 model can be also extended to mirrors with an off-axis focus: in
 204 that case the number of Zernike modes involved in the spot
 205 shaping is higher.

206 The identified modes are shown in 2D and 3D in Table 1.
 207 The deformation associated with the 4th mode (*defocus*) basically
 208 enlarges the image and contributes to spread the light quite
 209 similarly to the effect of shifting the receiver plane. The 11th
 210 mode (*third order spherical*) contributes to redistributing the
 211 rays maintaining an image radial symmetry and changing the
 212 image irradiance profile. These two polynomials do not have
 213 any impact on the spot shape since they have no azimuthal
 214 dependence. A deformation corresponding to the 14th polynomial
 215 (*vertical quadrafoil*) contributes to make a circular spot
 216 square along two preferential directions rotated 45 degree,
 217 depending on the coefficient sign. The effect of this specific
 218 deformation is less evident if the mirror is in focus mode: that
 219 is the reason for a combined use of the modes 14th and 4th.
 220 Alternatively, the same effect of this combination can be
 221 obtained by positioning the receiver slightly behind or above
 222 the correct focal plane and avoiding (partially or completely)
 223 the deformations related to the 4th mode. Since it is easier
 224 for a single mirror to produce a square uniform image when
 225 the defocus is bigger, this means that the lower the concentration
 226 factor the better the method works. The size of the spot to
 227 obtain depends on the desired concentration factor.
 228

229 A prescribed irradiance could be also obtained by employing
 230 this concept to design concentrators with several optimized
 231 mirrors focusing at the same receiver. In this case, the final
 232 illumination pattern impinging on the receiver would result in
 233 the sum of the incoherent illumination patterns produced by
 234 each single mirror, as we are going to show in the next sections.
 235

236 4. CASE OF A CPV DENSE ARRAY SYSTEM: DESIGN CHOICES

237
 238 A multi-mirror configuration can be useful to solve the issue
 239 of building a single huge mirror. In order to avoid a mosaic
 240 of hundreds reflective elements [15], we choose to design a
 241 CPV dish made by few monolithic mirrors mounted close together
 242 on the same structure. The selected configuration

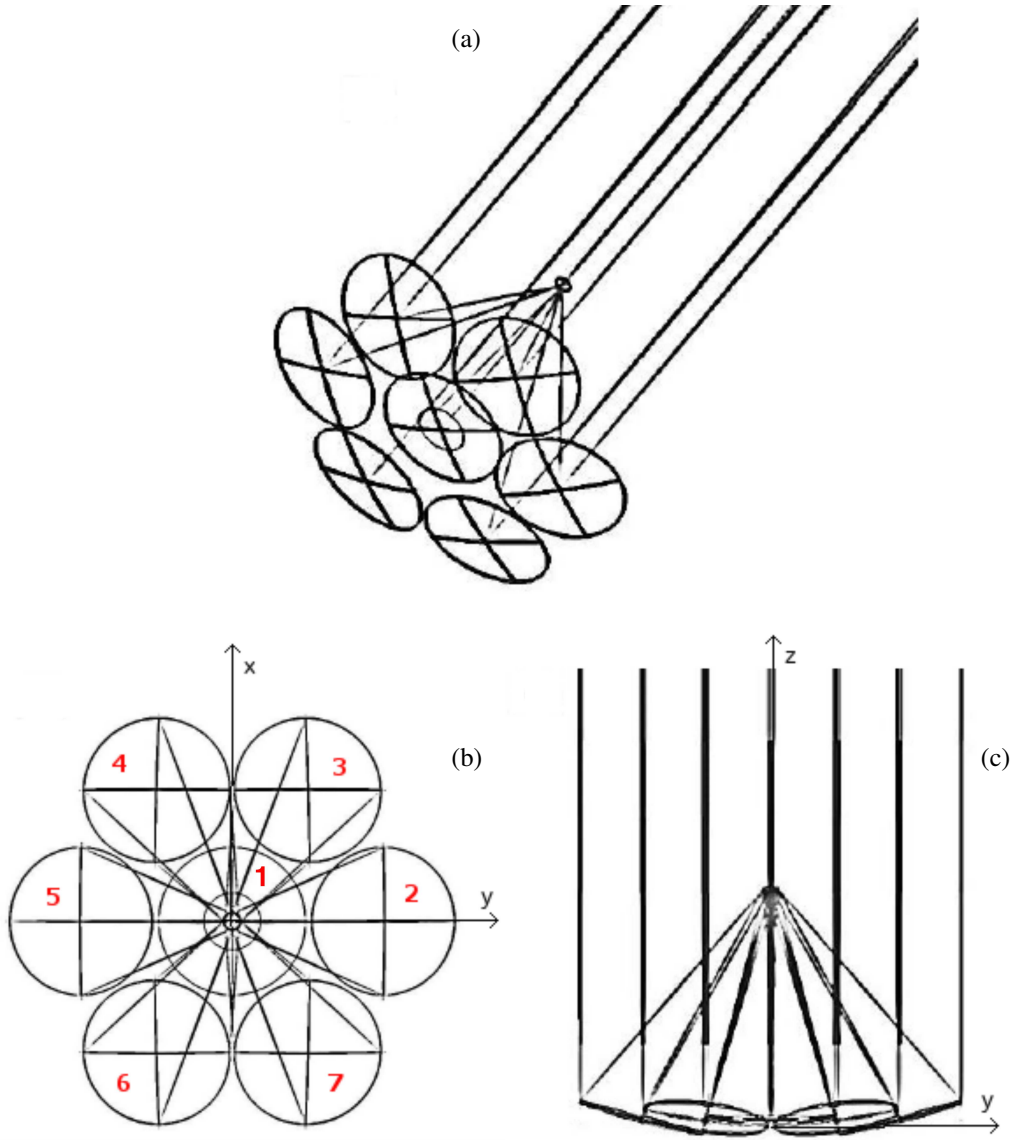


Figure 2: Optical layouts: a) 3D, b) x-y plane, c) y-z plane.

243 ration is the hexapolar grid and it has been already used in
 244 Stirling applications as well as in some ground based opti-
 245 cal telescopes. In the hexapolar configuration the elements
 246 are placed on rings so that the $(n+1)^{\text{th}}$ ring contains six el-
 247 ements more than the n^{th} ring, the central ring having only
 248 one element. We decided to consider only the central mir-
 249 ror and a ring of six mirrors arranged around it. Figure 2
 250 presents the optical layouts of the proposed system. The
 251 mirrors of the second ring have been labeled from 2 to 7
 252 counter-clockwise. The z-axis has been set as the direction
 253 of the incoming rays and it is perpendicular to the central
 254 mirror vertex. This optical condition of alignment with the
 255 solar direction should be the system nominal working state.

256 Considerations about the concentration ratio to be investi-
 257 gated and the mechanical compactness have been made also
 258 in comparison with similar existing prototypes and plants.
 259 Since this research activity has been carried out with the spe-
 260 cific goal of finding new solutions in the field of clean micro-

261 generated distributed electricity, our dish has been conceived
 262 as a power system suitable for the market of medium resi-
 263 dential contexts or small farms. We decided the mirror di-
 264 ameter to be around 2-3 meters, to avoid construction dif-
 265 ficulties. The diameter of the single mirror has been set to
 266 $D = 2600$ mm, for a total system size of about 7800 mm
 267 and a resulting total optical area slightly bigger than 35 m^2 .
 268 Supposing an irradiance at the collecting aperture of 1000
 269 W/mm^2 , the entry power would be around 35 KW: with a re-
 270 ceiver working almost at the efficiency of the best presently
 271 available cells (between 30%-40%), such a system would be
 272 able to deliver more than 10 KWe. Utility scale applications
 273 could be anyway considered, together with the scaling of the
 274 single elements for higher energy outputs.

275 The detector distance has been set to $h = 4800$ mm in or-
 276 der to have a low ratio of detector distance to total diameter.
 277 Considering this ratio similar to the focal ratio in imaging
 278 systems, a value $f/0.5$ should be approached to maximize

	Mirr1	Mirr2	Mirr3	Mirr4	Mirr5	Mirr6	Mirr7
X pos (mm)	0.00	0.00	2320.88	2320.88	0.00	-2320.88	-2320.88
Y pos (mm)	0.00	2680.00	1340.00	-1340.00	-2680.00	-1340.00	1340.00
α_x ($^\circ$)	0.00	-14.59	-7.41	7.41	14.59	7.41	-7.41
α_y ($^\circ$)	0.00	0.00	12.60	12.60	0.00	-12.60	-12.60
radius of curv. (mm)	10101.00	11480.10	11480.10	11480.10	11480.10	11480.10	11480.10

Table 2: Positions, tilt angles and curvatures of the seven mirrors.

the concentration but also to allow a more compact structure.

We investigated two concentration levels, $500\times$ and $800\times$. To obtain these concentrations, we applied a defocus to the mirrors which is the common method to modulate the concentration delivered at the receiver. A paraboloid in focus mode would have a collected flux too high for the cells working range (up to few thousands of suns at present). In our case, another reason to avoid extreme concentrations is that the deformations introduced by the Zernike modes are more efficient in reproducing the image features required when a defocus occurs.

The concentrator has been initially designed putting mirrors with the same diameter D on the same plane. The reference system has been chosen so that incoming rays are parallel to the z -axis, while the mirrors vertexes lay in the x - y plane. Each mirror has been placed at $d = 2680$ mm (in the x - y plane) from the central mirror vertex to prevent shading effects. The mirrors of the external ring have been tilted respect to the central one in order to focus all the chief rays from the Sun center at the center of the receiver plane having coordinates $(0, 0, h)$. This optical restriction is optional, but we aimed at simplifying the mechanical structure. The geometrical laws fulfilling this optical condition are easily derivable and once fixed the distance d in the hexapolar grid the positional/tilting parameters of the mirrors can be immediately calculated. The tilt of the external mirrors reduce by 5% the collecting projected area of the whole system from 37.17 m² to about 35.25 m². Positions, tilts and curvatures of the seven mirrors are listed in Table 2. The generic mirror surface sag has been described by Eq. 4.

5. DESIGN METHOD

To optically model our system, an end-to-end IDL[®] code has been written on purpose. Each step of the procedure and the results have been verified with the optical design software Zemax[®] as reference. The code includes four main subgroups of routines: the first for individually modeling the optical part; the second for the receiver implementation; the third for optimizing the optics; the last one for calculating tolerances of optical/mechanical parameters.

5.1 Optical Modeling

The initial optical parameters, which are the initial conditions of the simulations, have been set by a ray tracing anal-

ysis performed by Zemax[®]. The Sun has been modeled as a finite source with an angular diameter of 0.53° , neglecting its shape variations caused by the altitude changing during the day. The curvatures have been set so that the mirrors could produce a spot with a size compatible with the mean geometrical concentration chosen. The concentration ratio has been defined as the total mirrors area perpendicular to the axis of the central mirror divided by the total area of the receiver, supposing a receiver and a spot ideally with the same size. We ignored the obscuration introduced by the receiver itself.

The Zernike modes corresponding to deformations useful to fulfill our requirements of shape and uniformity have been selected after fixing the curvature. The deformations needed for the central mirror are the three described in paragraph 2, but other modes (from 5th to 8th) are necessary for the six off-axis mirrors. The selection criteria is that the superimposition of all the generated spots could produce an irradiance distribution with the desired features. Symmetry properties have been imposed for the six mirrors in the external ring to reduce the degrees of freedom of our problem. For example, these mirrors have been chosen with the same curvature radius and the same values of the 4th, 11th and 14th Zernike coefficients. As consequence, the non-zero coefficients are linked between mirrors by the geometrical relations shown in Table 3. In this way, opposite mirrors are equal but rotated by π and the final optical model results to be made of only four different types of surfaces. It could be certainly possible to identify more coefficients to improve the performance however increasing the complexity of the system. This condition would be more suitable both on construction and calibration stages. The independent modes identified for our system are eight, three for the central mirror (Z4(1), Z11(1) and Z14(1)) and five for the external ones, all derived from the modes of the mirror number 2 (Z4(2), Z6(2), Z7(2), Z11(2), Z14(2)) according to the relations shown in Table 3. The mirrors of the ring can not have all the same shapes even if this would be the best constructive condition. The 14th Zernike mode in fact corresponds to a deformation able to modify the circular symmetry of the ray bundle into a square and it has an azimuthal dependence. The simple rotation of a given surface would lead to a different analytical description in terms of its Zernike coefficients, except for the coefficients with pure radial dependence. This means that a ring generated by replicating mirror number 2 and simply rotating the replicas according to the position in the ring, would give a series of identical spot rotated as in Fig. 3a. The superimposition of these spots would certainly not lead

	Mirr1	Mirr2	Mirr3	Mirr4	Mirr5	Mirr6	Mirr7
Z4	Z4(1)	Z4(2)	Z4(2)	Z4(2)	Z4(2)	Z4(2)	Z4(2)
Z5	0.00	0.00	$-Z6(2) \cdot \cos 30^\circ$	$Z6(2) \cdot \cos 30^\circ$	0.00	$-Z6(2) \cdot \cos 30^\circ$	$Z6(2) \cdot \cos 30^\circ$
Z6	0.00	Z6(2)	$-Z6(2) \cdot \sin 30^\circ$	$-Z6(2) \cdot \sin 30^\circ$	Z6(2)	$-Z6(2) \cdot \sin 30^\circ$	$-Z6(2) \cdot \sin 30^\circ$
Z7	0.00	Z7(2)	$Z7(2) \cdot \sin 30^\circ$	$-Z7(2) \cdot \sin 30^\circ$	$-Z7(2)$	$-Z6(2) \cdot \sin 30^\circ$	$Z7(2) \cdot \sin 30^\circ$
Z8	0.00	0.00	$Z7(2) \cdot \cos 30^\circ$	$Z7(2) \cdot \cos 30^\circ$	$-Z7(2)$	$-Z6(2) \cdot \cos 30^\circ$	$-Z7(2) \cdot \cos 30^\circ$
Z11	Z11(1)	Z11(2)	Z11(2)	Z11(2)	Z11(2)	Z11(2)	Z11(2)
Z14	Z14(1)	Z14(2)	Z14(2)	Z14(2)	Z14(2)	Z14(2)	Z14(2)

Table 3: Correlation between the Zernike coefficients of the seven mirrors.

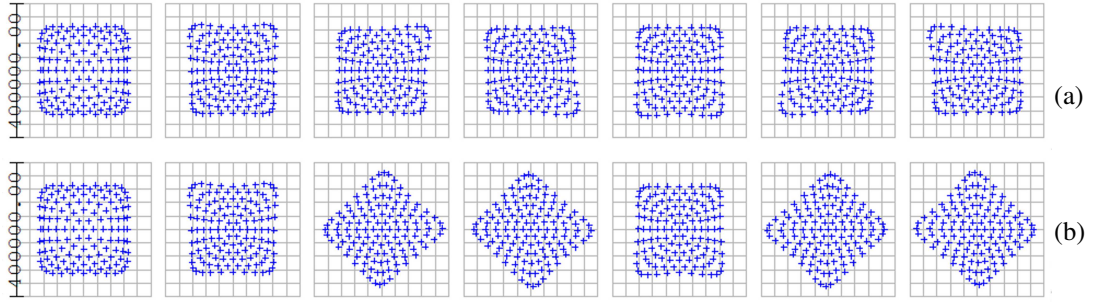


Figure 3: Effect introduced in the spot generated by each mirror by the introduction of a) a Z14 value rotated according to the mirror location and b) a common Z14 value.

370 to a final square shape. On the contrary, fixing the 14th coef-
371 ficient to the same value for all the surfaces, the features in
372 Fig. 3b are obtained. The physical size of the figure is $4 \cdot 10^5$
373 μm .

374 The optical scheme described is simulated by the ray-
375 tracing code written on purpose. The code output is the final
376 spot produced by the concentrator. In the algorithm, the con-
377 tinuous optical surfaces of the mirrors have been discretized
378 by a fixed number of sub-apertures. The rays striking every
379 sub-aperture are reflected toward the receiver according to
380 the classic reflection law. The Sun has been modeled as
381 an homogeneous circular source with a diameter of 0.53° ,
382 thus applying a realistic divergence model. The number of
383 rays traced from the Sun has been set in order to minimize
384 sampling errors. To calculate the nominal mirrors shape, we
385 supposed an ideal tracking condition in which the central solar
386 ray strikes the central mirror vertex parallel to the optical
387 axis.

Base Material	GaInP/GaAs/Ge on Ge substrate
AR Coating	TiOx/Al2Ox
Chip size	$5,59 \times 6,39 \text{ mm}^2 = 35,25 \text{ mm}^2$
Active Cell Area	$5,5 \times 5,5 \text{ mm}^2 = 30,25 \text{ mm}^2$

Table 4: Main features of the AZUR SPACE 3C40 cell implemented in the simulations.

5.2 Receiver Implementation

390 To simulate the performance of a dense array receiver, we
391 considered an electrical model for the PV cells. Neglecting
392 any temperature or spectral variation, the physical behavior

of a cell can be in first approximation summarized by the
following set of equations uniquely depending on the con-
centration factor \times :

$$I_{sc}(\times) = \times \cdot I_{sc}(1) \quad (5)$$

$$V_{oc}(\times) = V_{oc}(1) + n_d \frac{KT \ln(\times)}{q} \quad (6)$$

$$P_{max}(\times) = I_{max}(\times) \cdot V_{max}(\times) \quad (7)$$

$$FF(\times) = \frac{P_{max}(\times)}{I_{sc}(\times) \cdot V_{oc}(\times)} \quad (8)$$

$$\eta_{max}(\times) = \frac{P_{max}(\times)}{P_{in}(\times)} = I_{sc}(\times) \cdot V_{oc}(\times) \cdot \frac{FF(\times)}{P_{in}(\times)} \quad (9)$$

where P_{in} is the total power received by the cell and $I_{sc}(\times)$,
 $V_{oc}(\times)$ are short circuit current and open circuit voltage at
a given concentration, η_{max} is the nominal conversion effi-
ciency, n_d is the diode ideality factor, T is the absolute tem-
perature of the cell, K is the Boltzmann constant and q is
the electron charge. A more exhaustive model involving de-
pendences on T and spectral variations can be found in [42].
Equation 8 defines the Fill Factor FF as the ratio between
the power at the maximum power point P_{max} and the prod-
uct of the open circuit voltage and short circuit current. It is
typically better than 75% for good quality MJ solar cells. It
is also an index of the performance of a solar cell in terms
of generated power and it should be as close as possible to
100%: graphically, the FF is a measure of the *squareness*
of the solar cell $I - V$ curve and is also the area of the largest
rectangle which would fit in the curve.

Our receiver has been analytically designed and numeri-
cally simulated using a datasheet of commercially available
high concentration cells 3C40 produced by AZUR SPACE

	$I_{sc}(A)$	$V_{oc}(V)$	$I_{max}(A)$	$V_{max}(V)$	$P_{max}(W)$	$FF(\%)$	$\eta(\%)$
500×	2.151	3.144	2.102	2.842	5.98	88.0	39.0
1000×	4.239	3.170	4.135	2.762	11.42	85.0	37.8

Table 5: Electrical parameters of the AZUR SPACE 3C40 cell at 500× and 1000×.

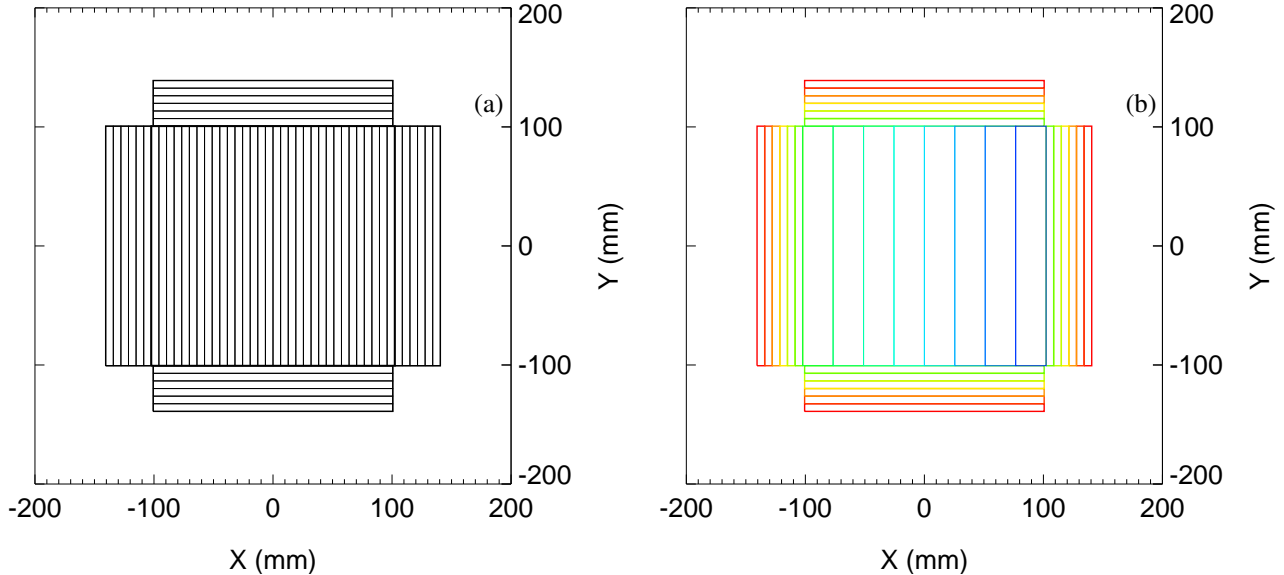


Figure 4: Type-3 receiver design at 500×. The a) panel shows the subdivision in strings. The b) panel shows which strings are series connected (zones with the same color). The 14 resulting blocks are parallel connected.

415 [44] with a nominal efficiency of 39% at 500× (around 38%
416 at 1000×) at ambient temperature. The reference cell has
417 main features described in Table 4.

418 In addition to efficiency, the cell datasheet gives other out-
419 put parameters (Table 5) necessary in the simulations to pre-
420 dict the cells power output at different illuminations. More-
421 over, since we deal exclusively with reflective elements, no
422 chromatic aberration are introduced. The temperature can
423 also be considered reasonably constant as efficient cooling
424 systems have been shown in literature.

425 The receiver electrical design has been chosen in order
426 to minimize the *power matching* problem even maintaining
427 high degree of linearity and easiness of construction: atten-
428 tion has been paid to series connected cells since the output
429 current in this case corresponds to the current produced by
430 the worst illuminated cells of the series.

431 The choice of the number of cells to connect has been
432 made starting from the concept that a receiver should have
433 a certain area to perform at a certain mean concentration.
434 The array design has to resemble, with the right connec-
435 tions, an irradiance distribution which is mostly square and
436 uniform and probably degrading toward the borders. To sim-
437 plify the scheme, we decided to simulate different receivers
438 starting from the same base unit, which is a string of ser-
439 ies connected cells. A scheme with many parallels would
440 lead to a lower dependence from irradiance gradients, but it
441 has the inconvenience to give high current and small volt-
442 ages in output. High voltages are instead more suitable for

443 the standard range of inverters while small currents limit the
444 resistive losses. We thus chose to conceptually design dif-
445 ferent receivers type to perform at different output voltages.
446 Figures 4a and 4b shows the third of the array implemented
447 for which we will show also the tolerance results. It is a
448 detector made by 56 strings of 36 cells. The strings spatial
449 positioning is shown in Fig. 4a where each string is repre-
450 sented by a narrow rectangle. There are 32 strings in the
451 central square zone, which corresponds roughly to the max-
452 imum uniform area obtainable by the optimization, and 4
453 lateral zones made by 6 additional modules each. The total
454 number of cells is 2016. This scheme allows cells in series
455 to be irradiated with similar fluxes and at the same time,
456 the strings and the groups contain the same number of elements
457 thus ensuring small parallel mismatches. This scheme does
458 not have cells at the corners, since the spillage losses in case
459 of 500× have been evaluated in the order of 5%. The elec-
460 trical connections are arranged as follows (Fig. 4b): cells in
461 each strings are series connected as well as strings with the
462 same color. The central zone is then made by 8 blocks of
463 cells each containing 4 adjacent substrings (the subdivision
464 of each colored areas have been omitted), while the lateral
465 strings are series connected in concentric frames. The 14
466 resulting blocks are finally parallel connected.

467 The same electrical scheme has been also used for simu-
468 lating the concentration 800×. In this case the cells of the
469 base string are only 27 and the central zone is made by 24
470 strings since the higher concentration results in a smaller ir-

radiated area. The parallel connected blocks are 12. Spillage losses at the corners are around 8-10% but again we preferred to preserve the array symmetry avoiding cells in these areas.

To analytically calculate the electrical performance, we developed a routine implementing the equations (5)-(9) modeling the cell output current and voltage as functions of concentration, neglecting resistive effects. As for the electrical scheme, the routine implements the classical equations for calculating voltages and currents in series and parallel connections. Only these connections are involved while no model has been implemented for the bypass diodes. A temperature of $T = 298$ K has been considered and a reasonable value for the ideality factor $n_d = 3.3$ has been assumed to treat the junctions as real. The other initial parameters used are in Table 5. Being FF only dependent on V_{oc} , it has been calculated using a classical empirical formula [43] approximated for zero resistivity:

$$FF(\times) = \frac{v_{oc}(\times) - \ln(v_{oc}(\times) + 0.72)}{1 + v_{oc}(\times)} \quad (10)$$

where $v_{oc}(\times)$ is the open circuit voltage normalized by the factor n_dKT/q .

5.3 Optimization procedure

The optimization procedure employs a downhill simplex method. We decided to minimize a merit function related to conversion efficiency. In particular it has been defined as the negative efficiency of the receiver $-\eta$ as defined in Eq. 9: each evaluation of this function requires the calculation of the efficiency by the ray tracing procedure and the receiver model previously explained. We summarize the optimization steps as follows.

The initial values chosen for the parameters to be optimized are inserted in the optimization routine. The routine operates performing a multidimensional minimization of a function $func(x)$ where x is an n-dimensional vector of parameters, using a downhill simplex method requiring only function evaluations and not derivatives. Additional input for the routine are the fractional tolerance to be achieved in the function value as well as the range of the parameters variation.

The optimization procedure transfers the parameters value to the ray-tracing procedures which gives the image as output, then the block simulating the receiver performance gets in input the image focused by the optics. The image is represented by a matrix containing the local concentration impinging on each receiver cell. The receiver model distinguishes between cells series and parallel connected, imposing the current of a series cells as the current produced by the

worst illuminated cell. Subsequently, the current and voltage output for each series/parallel are summed to give the total output and the efficiency. After calculating the efficiency of the optics coupled with that receiver, the procedure changes the parameters value iteratively in the range specified, modifying the optics and calculating a new image, a corresponding new efficiency and comparing the values of the simplex obtained. When the minimum is found within the threshold, the routine returns an n-element vector corresponding to the function minimum value. This kind of method could be applied to other type of receivers and it could be improved by extending the variables (for example the curvatures that here we considered fixed).

5.4 Tolerance calculation

After obtaining the nominal image produced by the optimized optics, a tolerance calculation has been implemented to assess the feasibility of the results. Tolerances have been obtained for both optical and geometrical parameters. We considered 25 parameters for each of the 4 different mirrors. Additional parameters are the two tracking angles and the receiver position along the z-axis, for overall 178 parameters. The parameters include tilts and positions of the mirrors, their curvatures and the Zernike coefficients up to the 6th radial order (from 4th to 21th). The reason for considering up to this order lays in the connection between the radial degree of the polynomials and the spatial scale of the deformations: the degree of a polynomial on a certain surface (which has a diameter of 2.6 m in the proposed design) roughly defines the spatial scale (period) of the associated deformation so that, for example, a 6th degree deformation on 2.6 m diameter would be roughly half meter ($2.6/6 \text{ m} = 0.43 \text{ m}$). It has been evaluated that higher degree deformations, i.e. occurring on spatial scales smaller than the considered scale, can be reasonably controlled by surface polishing of candidate materials (aluminum, molded plastics, etc.). The tolerances have been also calculated for polynomials with nominal null coefficients since all the polynomials up to a certain degree are necessary to model the irregularities down to a given scale.

The nominal image produced by the optics with the optimized parameters and the corresponding receiver efficiency have been calculated and stored as terms of comparison. We chose a range of variation for each parameter and a minimum tolerable efficiency. The tolerated efficiency degradation was equally split among all the parameters, assuming their effects as uncorrelated. Degraded efficiency has been calculated for the minimum and maximum values of a given parameter, keeping nominal values for all the other parameters: if the degraded efficiency is acceptable, the minimum

	Z4(1)	Z11(1)	Z14(1)	Z4(2)	Z6(2)	Z7(2)	Z11(2)	Z14(2)
500 ×	1.124	0.137	0.098	1.486	-0.616	0.223	0.003	-0.217
800 ×	1.103	0.070	-0.108	1.053	-0.714	0.280	0.019	-0.144

Table 6: Values in mm of the Zernike coefficients optimized at the two considered concentrations considering type-3 receivers.

566 and maximum values of the given parameter are adopted as
567 tolerances for that parameter, otherwise the variation range
568 of the parameter is reduced and the process is repeated until
569 convergence. After computing the tolerances for each pa-
570 rameter separately, the global effect has been evaluated by
571 perturbing all the parameters simultaneously in a random
572 fashion according to the computed tolerances and evaluat-
573 ing the corresponding efficiency.

574 6. RESULTS: THE SOLARIS CONCENTRA- 575 TOR

576 The results shown in Table 6 have been obtained by opti-
577 mizing our optics at two concentrations ($500\times$ and $800\times$)
578 with type-3 receivers. The values of the Zernike coefficients
579 not shown can be derived from the relations in Table 3.

580 The bi-dimensional and the x-cross section irradiance
581 produced by the optimized optics have been simulated by
582 Zemax[®] for the two concentration ratios and they are shown
583 in Fig. 5 and Fig. 6. The x-cross section irradiance is
584 evaluated on the central row parallel to the x-axis of the
585 bi-dimensional irradiance pattern. All the simulations have
586 been performed supposing 1 sun irradiance at the concen-
587 trator aperture, which is the common value in Standard Test
588 Conditions (STC).

589 The performance obtained for other receivers types de-
590 scribed in Section 5.2 are listed in Table 7. The efficiency
591 η is the output power of the receiver divided by the total
592 power collected by the optics. The optimized systems show
593 a conversion efficiency of about 30% in all the cases with
594 $500\times$ and of 28% in the only analysed case with $800\times$. The
595 case with higher concentration is interesting for the devel-
596 opment of new generation cells because it shows that the
597 proposed method gives good results also at higher concen-
598 trations. Moreover, the higher the concentration the smaller
599 the number of cells employed in the receiver. The case with
600 concentration $800\times$ in fact includes only 1152 cells, almost
601 half of the cells needed for the concentration $500\times$ (2016
602 elements).

603 The relative efficiency η_{rel} in Table 7 has been defined
604 considering the only effective power impinging on the array,
605 i.e. accounting for spillage losses at the corners/edges. This
606 parameter is useful to evaluate the average cells performance
607 in the array. In three of the four cases, its value is above 31%
608 and it must be compared with the maximum theoretical effi-
609 ciency reported in Section 5.2 for the active part of the cell
610 considered, i.e. 33% for concentration $500\times$ and 32% for
611 $1000\times$. This means that the cells in the arrays work really
612 close to their nominal performance under the irradiance pro-
613 duced by the optimized optics.

614 Looking at the results in Table 7 with concentration $500\times$,
615 the main difference between the three receivers analyzed
616 lays in the output parameters values. Even if the total power
617 produced is quite similar in all the cases (slightly higher than
618 10 KWe), the output current and voltage are very different.
619 The third receiver has been designed specifically with a high
620 number of series connections to obtain a high voltage value

(409.2 V) suitable for the available inverters and with small
621 current (25.3 A) to limit the resistive losses. This condition
622 is convenient from an electrical point of view, but it leads to
623 tighter tolerances, as shown below. 624

625 The tolerance results are here shown only for the concen-
626 tration $500\times$ with the type-3 receiver, giving some qualita-
627 tive indications for the other cases studied. The parameters
628 which differ from mirror to mirror are summarized in Tables
629 8 and 9 while the common parameters related to the receiver
630 position are shown in Table 10. Five out of seven mirrors
631 have been omitted from the list since their tolerances are
632 similar to those of the second mirror except for discretization
633 effects. The last row in Table 8 is the root square sum (RSS)
634 of the Zernike coefficients and it is one of the most important
635 tolerance indicators in our analysis since it represents the tol-
636 erated surface sag deviation. For all the mirrors, this param-
637 eter is in the order of tenths of a millimeter. The shape de-
638 viation tolerated is also compatible with the manufacturing
639 irregularities of candidate materials (molded plastics or alu-
640 minium) for the deformed/deformable mirrors. The tracking
641 errors shown in Table 10 are quite small if compared to other
642 CPV concentrators (normally in the order of 1 milliradian or
643 more). In any case, the tracking accuracy can be achiev-
644 able with standard tracking solutions commonly employed
645 in telescopes since these systems can also reach subarcsec-
646 onds tolerances. Good pointing and active tracking systems
647 are already developed also for solar concentrators [45], but
648 their performances should be further improved to allow our
649 tolerances.

650 The calculations have been performed setting a threshold
651 of 3% on the efficiency, i.e. tolerating a degradation of the
652 performance from 29.4% down to 26.4%. This value has
653 been chosen as reasonable for this type of systems, but it
654 can be varied depending on the required performance. In
655 general, for small perturbations, the tolerance on a parameter
656 scales linearly with the threshold value. The tolerances are
657 strictly related to the electrical scheme implemented in the
658 receiver. For example we calculated that with the receiver
659 involving more parallels and with the same threshold, the
660 tolerances would be three times more relaxed. In that case
661 higher output current would be produced, the output power
662 being approximately the same.

663 The mechanical model is shown in Fig. 7. From the anal-
664 ysis of the Zernike polynomials, the desired deformations on
665 the mirrors can be applied by a restricted number of actua-
666 tors positioned on a certain number of control points. For the
667 system with the chosen dimensions, these points are located
668 radially on three circumferences every 10° . A possible way
669 to obtain the final surfaces is to use spherical mirrors and to
670 set the deformations by the actuators. Another approach is to
671 freeform mirrors already shaped with the final form desired,
672 the actuators being employed only to compensate the shape
673 errors once the mirrors have been placed on their own sup-
674 port. All these mirrors could be made by aluminum sheets,
675 since this material is particular suitable for its lightness and
676 its ductility. Molded plastic could be also a candidate sub-
677 strate material (if compatible with the requested tolerances)
678 after the deposition of a high reflective layer. During the

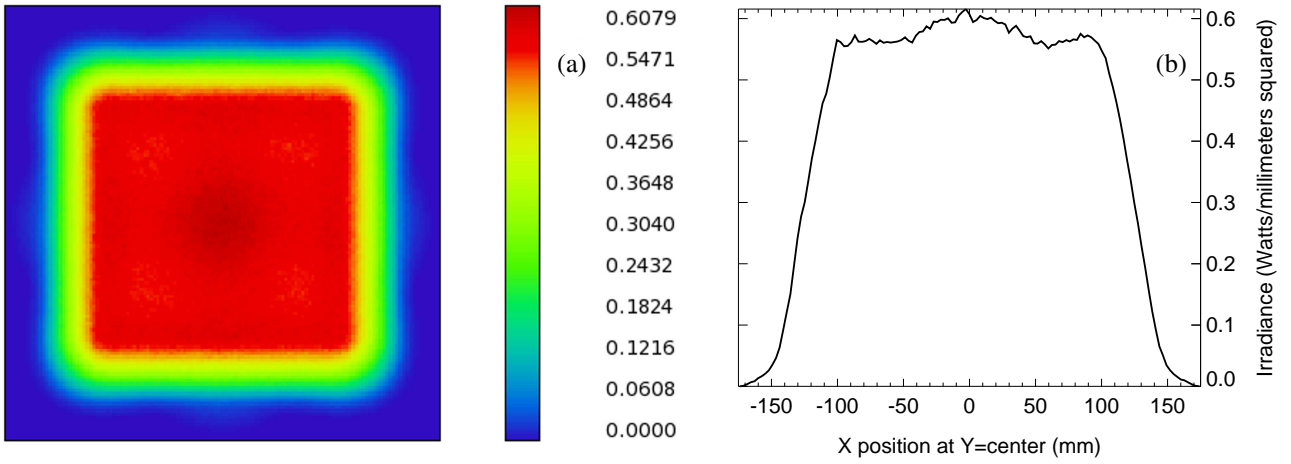


Figure 5: a) 2D and b) x-cross section irradiance produced by the optics coupled to the type-3 designed for 500 \times . The physical size of the figures is 350 mm. Units in the color bar are Watt/mm².

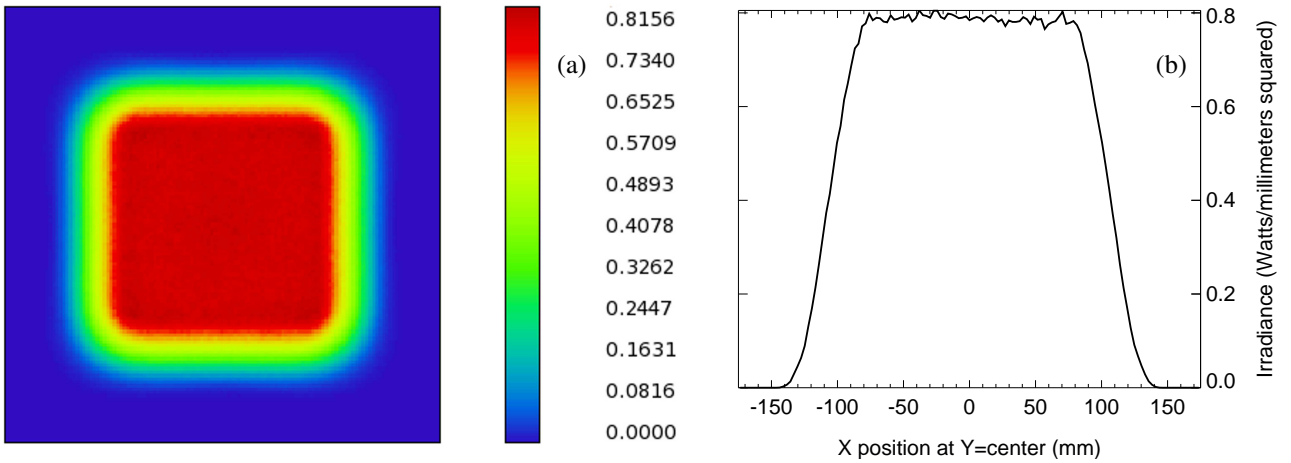


Figure 6: a) 2D and b) x-cross section irradiance produced by the optics coupled to the type-3 designed for 800 \times . The physical size of the figures is 350 mm. Units in the color bar are Watt/mm².

	$I_{out}(A)$	$V_{out}(V)$	$P_{out}(W)$	$\eta(\%)$	$\eta_{rel}(\%)$
Receiver 1 (500\times)	98.7	105.2	10288.0	29.2	30.5
Receiver 2 (500\times)	50.5	204.6	10324.8	29.7	31.6
Receiver 3 (500\times)	25.3	409.2	10354.5	29.4	31.2
Receiver 3 (800\times)	32.6	302.6	9868.1	28.0	31.4

Table 7: Electrical performance obtained after the optimization run with the three receivers implemented.

Units	Parameter	Mirr1		Mirr2		
		nominal value	tolerance	nominal value	tolerance	
mm	Z4	1.124	0.063	1.486	0.063	
	Z5	0.000	0.063	0.000	0.031	
	Z6	0.000	0.250	-0.616	0.063	
	Z7	0.000	0.031	0.223	0.016	
	Z8	0.000	0.031	0.000	0.016	
	Z9	0.000	0.031	0.000	0.031	
	Z10	0.000	0.031	0.000	0.016	
	Z11	0.137	0.008	0.003	0.016	
	Z12	0.000	0.016	0.000	0.008	
	Z13	0.000	0.016	0.000	0.008	
	Z14	0.098	0.016	-0.217	0.031	
	Z15	0.000	0.016	0.000	0.016	
	Z16	0.000	0.016	0.000	0.004	
	Z17	0.000	0.004	0.000	0.008	
	Z18	0.000	0.016	0.000	0.008	
	Z19	0.000	0.008	0.000	0.008	
	Z20	0.000	0.016	0.000	0.016	
	Z21	0.000	0.016	0.000	0.008	
	mm	$\sqrt{\sum Z^2}$	0.2762		0.1122	

Table 8: Zernike coefficients tolerances calculated for the system with 500× coupled with a type-3 receiver.

Units	Parameter	Mirr1		Mirr2	
		nominal value	tolerance	nominal value	tolerance
mm	radius of curv.	10101.0	25.0	11480.1	25.0
mrad	tilt x	0.0	0.4	-254.6	0.2
	tilt y	0.0	0.9	0.0	0.1
	tilt z	0.0	1.7	0.0	1.7
mm	offset x	0.0	5.0	0.0	2.5
	offset y	0.0	2.5	2680.0	2.5
	offset z	0.0	25.0	0.0	3.1

Table 9: Tolerances on other parameters calculated for the system with 500× coupled with a type-3 receiver.

679 realization, the system should be aligned within tolerances.
680 For this reason, we conceived a 2-step procedure. The first
681 phase consists in the mirrors positioning on their own sup-
682 ports and the calibration of their nominal shape. This test
683 can be performed in laboratory and it requires a point light
684 source, a beam splitter, a Shack-Hartmann (SH) wavefront
685 sensor [46] with a camera. The camera acquires the image
686 of a point source reflected back by the mirror which can be
687 used to recognize the wavefront shape and the mirror surface
688 map. The actuators are tuned iteratively until the measured
689 surface map matches its nominal value (within tolerances,
690 see Tables 9 and 10). To accelerate the calibration proce-
691 dure, an interaction matrix records the SH sensor reaction
692 to the specific movement of each single actuator. This ma-
693 trix has to be inverted and used to transform the SH sensor
694 signal into incremental corrections to apply to the actuators.
695 The second stage is an alignment on Sun of each mirror on
696 the whole frame. A mask dimensioned as the receiver and
697 realized in a material resistant to temperatures of a few hun-
698 dreds degrees is needed. Concentric frames of pinholes on

699 the mask transmit part of the light impinging on the receiver
700 plane to diodes or other electronic light-sensitive devices.
701 Such a tool allows to sample the irradiance distribution pro-
702 duced by the optics and to adjusted iteratively the position
703 of each mirror on the common frame until the desired ir-
704 radiance is obtained. Another interaction matrix is used to
705 record the diodes reaction to the parameters to align. This
706 matrix is then inverted and used to translate the measured
707 signal into corrections for the mirror positioning.

708 The new concentrator resulting from the investigation car-
709 ried out has been called "SOLARIS (SOLAR Image Squar-
710 ing) Concentrator" and it has been patented in Italy. The
711 patent is owned by both the University of Bologna and the
712 National Institute of Astrophysics (INAF), the two research
713 institutes involved in the project. Main subjects of the patent
714 are both the innovative concentrating CPV application and
715 the method for the numerical optimization of reflective sur-
716 faces. The procedures to test/calibrate the reflective shapes
717 and to align the mirrors on Sun, as well as the receiver and
718 the mechanical design are all parts of the patent. The model

Units	Parameter	All Mirrors	
		nominal value	tolerance
mrad	tracking error x	0.0	0.11
	tracking error y	0.0	0.01
mm	receiver offset z	4800.0	2.5

Table 10: Tolerances calculated for to the common parameters.

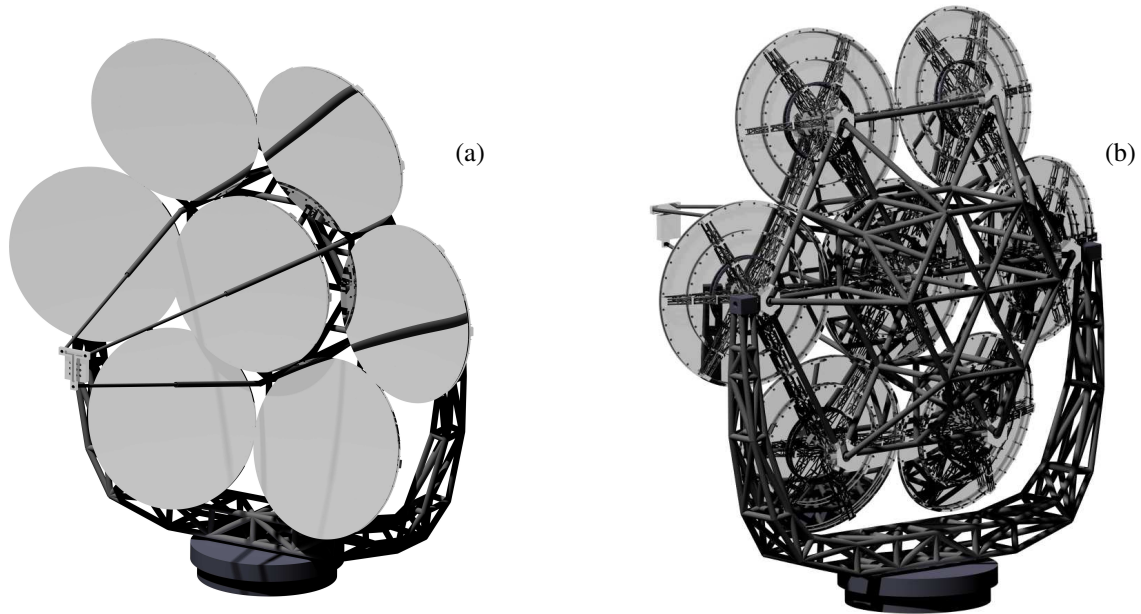


Figure 7: Shaded models of the SOLARIS Concentrator: a) front side, b) rear side.

719 and the obtained results will be validated with the described
720 procedures during the forthcoming prototyping stage.

721 SUMMARY AND DISCUSSION

722 We developed a new optical designing method for solar
723 concentrators. In particular, dense array photovoltaic appli-
724 cations need an accurate control on both shape and irradiance
725 of the collected light spot to perform at high efficiency.
726 These systems are experiencing in the last years growing inter-
727 est (from market and research) as feasible solutions in the
728 production of cost competitive electricity on demand, espe-
729 cially in very sunny environments and off-grid communi-
730 ties. The development of solar cells that can work at very
731 high irradiance imposes a technological jump also from an
732 optical point of view, to let these systems work at the same
733 performance of the employed cells. The proposed method
734 is based on controlling the optical shapes so that the spot
735 produced by the mirrors can resemble the optimal features
736 for the chosen receiver without including secondary optics.
737 The deformations to apply have been analytically modelled
738 by the Zernike polynomials and the deformed mirrors have
739 been simulated by ray tracing routines developed on pur-
740 pose. At the same time, different schemes of dense array re-
741 ceivers have been designed using reference cells with known

742 features and simulated by implementing simple electrical
743 models for photovoltaic devices. The deformed optics have
744 been numerically optimized to maximize the performance of
745 the concentrator as a function of the coupled receiver. The
746 method has been fruitfully employed to solve the prescribed
747 irradiance problem at high concentration in CPV dishes. It
748 has led to the design of a novel CPV optics, the SOLARIS
749 concentrator. Both the method implemented and the specific
750 application developed have been patented in Italy.

751 The main advantage of using big monolithic mirrors is
752 to have few optics to manage respect to the complex seg-
753 mented optics proposed in other researches involving dense
754 arrays. Despite this technology is quite recent and commer-
755 cial plants are not as diffused as the refractive fresnel lens
756 based systems, our method to design dense array concentra-
757 tors opens a new scenario for developing PV systems that
758 could perform at very high efficiency working at high con-
759 centrations. This efficiency boosting up to nominal levels
760 and, at the same time, the relaxation of the constraints on the
761 receiver design and the recent development of new materi-
762 als for optical application suggest interesting perspectives of
763 cost reduction.

764 The concentrator developed is a single stage multi-mirror
765 system made by 7 monolithic optics placed in an hexapolar
766 arrangement and all focusing on the same receiver. The
767 principal investigated design has a mean concentration ra-

768 tio $500\times$. The deformations applied to the optics allow
 769 them to produce a solar spot resembling a square shape
 770 with smoothed corners. The irradiance pattern inside the
 771 spot obtained is highly uniform. At this concentration, the
 772 optimized optics can boost the conversion efficiency of the
 773 whole receiver up to 30%, almost the same theoretical per-
 774 formance of the single cell used in the calculations which
 775 is around 33% (considering only the active areas). The re-
 776 ceiver has been designed as simple as possible, using exclu-
 777 sively strings of identical cells in series. The strings are then
 778 organized in parallels or series connections, with a Cartesian
 779 configuration and not involving bypass diodes in the design.

780 From an optical point of view, different considerations can
 781 been made to extend the purposes and the applications of
 782 the method conceived. Similar systems with different con-
 783 centrations can be surely designed ever keeping in mind the
 784 optimization method has been tested for the two concentra-
 785 tion $500\times$ and $800\times$, and that the results are better in the
 786 first case considered thanks to the higher defocus involved.
 787 Despite this, we demonstrated that our method can work ef-
 788 ficiently also at many hundreds of concentration ratio.

789 Method improvements could be done by a further investi-
 790 gation of the convenient deformations to introduce, explor-
 791 ing for example the effects related to Zernike polynomials
 792 of higher degrees. The selected deformations and the opti-
 793 cal configuration used in this work are indeed only an ex-
 794 ample of the method proposed: other concentrators could
 795 be designed by adding deformations or changing the geo-
 796 metrical/optical parameters as a function of the desired spot
 797 features. Systems with single or multiple mirrors (differ-
 798 ent or not) could be implemented and different geometrical
 799 configurations explored. Also the mirrors aperture could be
 800 varied in shape and size depending on the amount of output
 801 power needed or on the economical/constructive constraints.
 802 The final spot could result from a superimposition of images
 803 not necessarily centered in the same point, as in the stud-
 804 ied cases. Another interesting application could result from
 805 exploring the performance of deformable optics including
 806 very simple reflective secondary optics to recover possible
 807 light losses at the receiver borders or to relax the tolerances
 808 (thus enhancing the acceptance angle).

809 A great advantage of employing actively deformable op-
 810 tics could be given by the tuning of the concentration ra-
 811 tio. Using convenient deformable materials, flexible systems
 812 could be obtained embedding different type of receivers but
 813 exploiting the same optics. Also from the receiver point
 814 of view, great improvements could be obtained in terms of
 815 electric efficiency, involving optimized electrical schemes or
 816 thinking to future monolithic receivers. Finally, an exten-
 817 sion of this method could be also helpful in solving thermal
 818 problems. Thermal concentrators do also need a certain uni-
 819 formity in the light collected to optimally transfer the en-
 820 ergy to the exchanging fluid. The proposed technique could
 821 be implemented to correct possible optical aberrations thus
 822 boosting the concentration up to its limit.

ACKNOWLEDGEMENTS

This research activity has been financially supported by a
 MIUR PhD grant and a Fondazione CARISBO grant within
 the research framework on renewable sources, energy spare
 and distributed micro-generation.

REFERENCES

- [1] Green MA, Emery K, Hishikawa Y, Warta W, Dunlop ED. Solar cell efficiency tables (version 42). *Prog. Photovolt: Res. Appl.* 2013; **21**: 827-837. doi:10.1002/pip.2404
- [2] Wiesenfarth M, Hilmers H, Philipps SP, Steiner M, Bett AW. Advanced concepts in concentrating photovoltaics (CPV). *Proc. of 27th European Photovoltaic Solar Energy Conference and Exhibition 2012*, Frankfurt, Germany: 11-15. doi:10.4229/27thEUPVSEC2012-1AP.1.4
- [3] Benítez P, Miñano J, Zamora P, Moledano R et al. High performance Fresnel-based photovoltaic concentrator. *Opt. Express* 2010; **18**: A25-A40. doi:10.1364/OE.18.000A25
- [4] Singh PL, Sarviya RM, Bhagoria JL. Thermal performance of linear Fresnel reflecting solar concentrator with trapezoidal cavity absorbers. *Applied Energy* 2010; **87**(2): 541-550. doi:10.1016/j.apenergy.2009.08.019
- [5] Ryu K, Rhee JG, Park KM, Kim J. Concept and design of modular Fresnel lenses for concentration solar PV system, *Solar Energy* 2006; **80**(2): 1580-1587. doi:10.1016/j.solener.2005.12.006
- [6] Leutz R, Suzuki A, Akisawa A, Kashiwagi T. Design Of A Nonimaging Fresnel Lens For Solar Concentrators. *Solar Energy* 1999; **65**(6): 379-387. doi:10.1016/S0038-092X(98)00143-1
- [7] Feuermann D, Gordon J. High-concentration photovoltaic designs based on miniature parabolic dishes. *Solar Energy* 2001; **70**(5): 423-430. doi:10.1016/S0038-092X(00)00155-9
- [8] Kribus A, Kaftori D, Mittelman G, Hirshfeld A et al. A miniature concentrating photovoltaic and thermal system. *Energy Conversion and Management*; **47**(20): 3582-3590. doi:10.1016/j.enconman.2006.01.013
- [9] Gordon JM, Katz EA, Eugene A, Feuermann D, Mahmoud H. Toward ultrahigh-flux photovoltaic concentration. *Applied Physics Letters* 2004; **84**: 3642-3644. doi:10.1063/1.1723690
- [10] <http://www.apollon-eu.org>
- [11] Kinsey GS, Sherif RA, Cotal HL, Pien P et al. Multijunction Solar Cells for Dense-Array Concentrators. *Proc. of the IEEE 4th World Conf. on Photovoltaic Energy Conversion 2006*: 625-627. doi:10.1109/WCPEC.2006.279532
- [12] Verlinden P, Lewandowski A, Bingham C, Kinsey G, Sherif R, Lasich J. Performance and Reliability of Multijunction III-V Modules for Concentrator Dish and Central Receiver Applications. *Proc. of the IEEE 4th World Conf. on Photovoltaic Energy Conversion 2006*: 592-597. doi:10.1109/WCPEC.2006.279526

- 875 [13] Chayet H, Kost O, Moran R, Lozovsky I. Efficient, Low
876 Cost Dish Concentrator for a CPV Based Cogeneration Sys-
877 tem. *AIP Conference Proceedings* 2011; **1407**: 249-252.
878 doi:10.1063/1.3658337
- 879 [14] Lasich JB, Verlinden PJ, Lewandowski A, Edwards D
880 et al. World's first demonstration of a 140kWp Heliostat
881 Concentrator PV (HCPV) system. *34th IEEE Photovoltaic
882 Specialists Conference (PVSC) 2009*: 002275,002280.
883 doi:10.1109/PVSC.2009.5411354
- 884 [15] Chong KK, Siaw FL. Electrical Characterization of Dense-
885 Array Concentrator Photovoltaic System. *27th European
886 Photovoltaic Solar Energy Conference* 2012; Frankfurt, Ger-
887 many. doi:10.4229/27thEUPVSEC2012-1AV.3.18
- 888 [16] Minuto A, Timo G, GropPELLI P, Sturm M. Concentrating
889 photovoltaic multijunction (CPVM) module electrical lay-
890 out optimisation by a new theoretical and experimental mis-
891 match analysis including series resistance effect. *35th IEEE
892 Photovoltaic Specialists Conference (PVSC) 2010*; 003081-
893 003086. doi:10.1109/PVSC.2010.5614540
- 894 [17] Cooper T, Pravettoni M, Cadruvi M, Ambrosetti G, Ste-
895 infeld A. The effect of irradiance mismatch on a semi-
896 dense array of triple-junction concentrator cells. *Solar En-
897 ergy Materials and Solar Cells* 2013; **116**: 238-251.
898 doi:10.1016/j.solmat.2013.04.027
- 899 [18] Luque A, Sala G, Arboiro JC. Electric and thermal model
900 for non-uniformly illuminated concentration cells. *Solar En-
901 ergy Materials and Solar Cells* 1998; **51**(3-4): 269-290.
902 doi:10.1016/S0927-0248(97)00228-6
- 903 [19] Franklin E, Coventry J. Effects of highly non-uniform illu-
904 mination distribution on electrical performance of solar cells.
905 *Proc. Solar Australian and New Zealand Solar Energy Soci-
906 ety* 2003
- 907 [20] Katz EA, Gordon JM, Feuermann D. Effects of ultra-
908 high flux and intensity distribution in multi-junction solar
909 cells. *Prog. Photovolt: Res. Appl.* 2006; **14**(4): 297-303.
910 doi:10.1002/pip.670
- 911 [21] Herrero R, Victoria M, Domínguez C, Askins S, Antón I,
912 Sala G. Concentration photovoltaic optical system irradiance
913 distribution measurements and its effect on multi-junction
914 solar cells. *Prog. Photovolt: Res. Appl.* 2012; **20**(4): 423-
915 430. doi:10.1002/pip.1145
- 916 [22] Hernández M, Cvetkovic A, Benítez P, Miñano JC. High-
917 performance Kohler concentrators with uniform irradi-
918 ance on solar cell. *Proc. SPIE 7059, Nonimaging Optics
919 and Efficient Illumination Systems V* 2008; n.705908.
920 doi:10.1117/12.794927
- 921 [23] Fu L, Leutz R, Annenn HP. Evaluation and comparison of
922 different designs and materials for Fresnel lens-based solar
923 concentrators. *Proc. SPIE 8124, Nonimaging Optics: Effi-
924 cient Design for Illumination and Solar Concentration VIII*
925 2011; n.81240E. doi:10.1117/12.893390
- 926 [24] Leutz R, Suzuki A, Akisawa A, Kashiwagi A. Flux unifor-
927 mity and spectral reproduction in solar concentrators using
928 secondary optics. *ISES Solar World Congress* 2001; Adelaide
- [25] Baig H, Heasman KC, Mallick TK. Non-uniform il- 929
lumination in concentrating solar cells. *Renewable and* 930
Sustainable Energy Reviews 2012; **16**(8): 5890-5909. 931
doi:10.1016/j.rser.2012.06.020 932
- [26] Salemi A, Eccher M, Miotello A, Brusa RS. Dense array 933
connections for photovoltaic systems. *Prog. Photovolt: Res.* 934
Appl. 2011; **19**(4): 379-390. doi:10.1002/pip.1040 935
- [27] Loeckenhoff R, Kubera T, Rasch KD. Water Cooled TJ 936
Dense Array Modules for Parabolic Dishes. *AIP Conference* 937
Proceedings 2010; **1277**: 43-46. doi: 10.1063/1.3509229 938
- [28] Vivar M, Antón I, Sala G. Radial CPV receiver. *Prog. Photo-* 939
volt: Res. Appl. 2010; **18**(5): 353-362. doi: 10.1002/pip.921 940
- [29] Chong KK, Wong CW, Siaw FL, Yew TK. Optical Charac- 941
terization of Nonimaging Planar Concentrator for the Appli- 942
cation in Concentrator Photovoltaic System. *J. Sol. Energy* 943
Eng 2010; **132**(1) n. 011011. doi:10.1115/1.4000355 944
- [30] Siaw FL, Chong KK, Wong CW. A comprehensive study 945
of dense-array concentrator photovoltaic system using non- 946
imaging planar concentrator. *Renewable Energy* 2014; **62**: 947
542-555. doi: 10.1016/j.renene.2013.08.014 948
- [31] Riveros-Rosas D, Sánchez-González M, Arancibia-Bulnes 949
CA, Estrada CA. Influence of the size of facets on point fo- 950
cus solar concentrators. *Renewable Energy* 2011; **36**(3): 966- 951
970. doi:10.1016/j.renene.2010.08.038 952
- [32] Tan MH, Chong KK, Wong CW. Optical characterization of 953
nonimaging dish concentrator for the application of dense- 954
array concentrator photovoltaic system. *Appl. Opt.* 2014; 955
53(3): 475-486. doi:10.1364/AO.53.000475 956
- [33] Bianchi M, Diolaiti E, Giannuzzi A, Marano B, Melino F. 957
Energetic and Economic Analysis of a New Concept of Solar 958
Concentrator for Residential Application. *Energy Proce-* 959
edia, in Proc. of the 7th International Conference on Applied 960
Energy ? ICAE 2015; Abu Dhabi, United Arab Emirates 961
- [34] Wilson RN, Franza F, Noethe L. Active Optics I: A system 962
for optimizing the optical quality and reducing the costs of 963
large telescopes. *Journal of Modern Optics* 1987; **34**(4): 485- 964
509 965
- [35] Noethe L, Franza F, Giordano P, Wilson RN et al. Active 966
Optics II. Results of an Experiment with a Thin 1 m Test 967
Mirror. *Journal of Modern Optics* 1988; **35**(9): 1427-1457. 968
doi:10.1080/09500348814551591 969
- [36] Biasi R, Gallieni D, Salinari P, Riccardi A, Mantegazza P. 970
Contactless thin adaptive mirror technology: past, present, 971
and future. *Proc. SPIE - Adaptive Optics Systems II* 2010; 972
7736. doi:10.1117/12.858816 973
- [37] Angel R, Connors T, Davison W, Olbert B, Sivanandam S. 974
New architecture for utility-scale electricity from concentra- 975
tor photovoltaics. *Proc. of SPIE - The International Society* 976
for Optical Engineering 2010; 7769 977
- [38] Steeves J, Pellegrino S. Ultra-Thin Highly Deformable Com- 978
posite Mirrors. *54th AIAA/ASME/ASCE/AHS/ASC Struc-* 979
tures, Structural Dynamics, and Materials Conference 2013 980

- 981 [39] Ning X, Pellegrino S. Design of lightweight struc-
982 tural components for direct digital manufacturing. *53rd*
983 *AIAA/ASME/ASCE/AHS/ASC Structures, Structural Dynam-*
984 *ics and Materials Conference 2012*
- 985 [40] Irschik H. A review on static and dynamic shape control of
986 structures by piezoelectric actuation. *Engineering Structures*
987 2002; **24**(1): 5-11. doi:10.1016/S0141-0296(01)00081-5
- 988 [41] Noll R. Zernike polynomials and atmospheric tur-
989 bulence. *J. Opt. Soc. Am.* 1976; **66**(3): 207-211.
990 doi:10.1364/JOSA.66.000207
- 991 [42] Domínguez C, Antón I, Sala G. Multijunction solar cell
992 model for translating I-V characteristics as a function of ir-
993 radiance, spectrum, and cell temperature. *Prog. Photovolt:*
994 *Res. Appl.* 2010; **8**(4): 272-284. doi:10.1002/pip.965
- 995 [43] Green MA. Solar cell fill factors: General graph and empir-
996 ical expressions. *Solid-State Electronics* 1981; **24**(8): 788-
997 789. doi:10.1016/0038-1101(81)90062-9
- 998 [44] <http://www.azurspace.com>
- 999 [45] Fontani D, Sansoni P, Francini F, Jafrancesco D et
1000 al. Pointing sensors and sun tracking techniques. *In-*
1001 *ternational Journal of Photoenergy* 2011; n. 806518.
1002 doi:10.1155/2011/806518
- 1003 [46] Shack RV, Platt BC. Production and use of a lenticular Hart-
1004 mann screen. *J. Opt. Soc. Am.* 1971; **61**(5): 656-660.